Corrosion-induced cracking and bond strength in reinforced concrete

Corrosion-induced cracking and bond strength in reinforced concrete

Michele Win Tai Mak [1a], Pieter Desnerck[a], Janet M. Lees[a]

[a]*Department of Engineering, University of Cambridge, Trumpington St, Cambridge CB2 1PZ, United Kingdom*

Abstract

Corrosion of the steel reinforcement is among the main causes of deterioration in concrete structures. Measures of corrosion levels are typically used to evaluate the subsequent reduction in steel-to-concrete bond, but results lack accuracy. In this study, a new assessment approach based on surface cracks was investigated. Specimens were subjected to accelerated corrosion using an impressed current. With a novel sealing method, mass losses were decoupled from concrete cracking. The results indicate that surface crack widths can be better indicators of bond degradation than corrosion levels. The findings can lead to more accurate assessments and reduced maintenance costs of infrastructure.

Keywords:
assessment, bond, carbonation, chloride, corrosion, crack, degradation, deterioration, inspection, rust

1. Introduction

The deterioration of civil structures is a major concern that affects the safety, maintenance cost and environmental footprint of the infrastructure network [1, 2, 3]. For instance, a study published by the American Society of Civil Engineers (ASCE) in 2017 [4] estimated the overall cost for the rehabilitation of bridges in the United States to be US$123 billion, indicating the large scale of the problem. In effective asset management strategies, accurate structural assessments are crucial to avoid unnecessary costly interventions while safeguarding the safety of the community. However, it is currently challenging to quantify with accuracy the effects of deterioration mechanisms that are not directly visible. This is typically the case for reinforced concrete.

Concrete structures are subjected to several sources of deterioration that can reduce their load-bearing capacity. In particular, corrosion of the internal steel reinforcement is widely considered to be one of the most critical deterioration mechanisms [5, 6, 7, 8, 9, 10, 11, 12, 13, 14, 15, 16, 2, 3]. Corrosion affects the overall structural capacity in different ways. It leads to a reduction of the cross section of a steel bar, directly reducing the maximum tensile force that the bar can resist. As corrosion products occupy a greater volume than the parent metal, they develop expansive pressures. Low levels of corrosion may enhance the bond strength, but at higher levels it can lead to cracking of the surrounding concrete [5, 6, 17, 18, 16]. As the longitudinal cracks open, the contact area between the concrete lugs and the steel ribs is reduced (see Fig. 1), compromising the load-transfer capacity. Corrosion products also weaken the interface between steel and concrete by reducing the cohesion and friction between the two materials. General corrosion often

[1]Corresponding author. Email: mwtm2@cam.ac.uk

affects the bond strength before the reduction in the bar cross section has a significant impact on the tensile capacity of the bar [17, 19]. In fact, distributed mass losses due to corrosion that are critical for bond can be lower than the acceptable fabrication tolerances of reinforcing bars [5, 17]. For reference, the BS 4449:2005+A3:2016 [20] indicates a maximum permissible deviation from nominal mass of ±4.5% for nominal diameters greater than 8 mm and ±6.0% for nominal diameters less than or equal to 8 mm. As a result of bond deterioration, the steel-concrete composite action and the reinforcement anchorage are compromised, causing a reduction of the overall structural capacity. A comprehensive overview of the effects of reinforcement corrosion and bond reduction is given in fib Bulletin 10 [17].

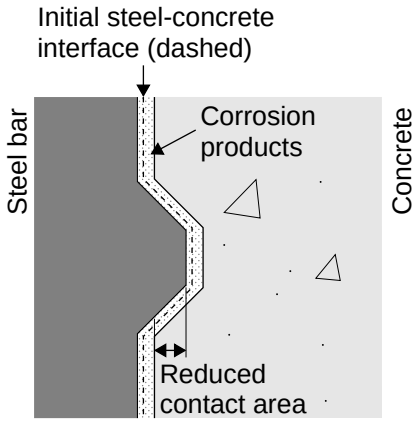

Figure 1: Effect of corrosion on the interlock between reinforcement ribs and concrete lugs. Reduction in contact area.

Although much research has been devoted to the mechanical effects of corrosion in concrete, several aspects are still the subject of scientific debate. Reinforcement corrosion has been studied under natural conditions, through controlled exposure to contaminants (typically chlorides), or with accelerated corrosion using an impressed current. In all cases, it is widely accepted that the current density i_{corr} is a key parameter in the corrosion process [21, 17, 22, 7, 23] and the appropriate values for laboratory experiments is at the centre of a lot of unresolved scientific discussion. The current density is defined as the average current intensity I involved in the electrochemical process divided by the steel surface area exposed to corrosion A_r:

$$i_{corr} = \frac{I}{A_r} = \frac{I}{\pi \cdot \varnothing \cdot l_b} \tag{1}$$

where the exposed surface area is calculated using the nominal diameter of the bar $\varnothing$ over the corroding length l_b. In reinforced concrete structures that are in service, current densities in the passive state are typically below 0.1μA/cm^2. In the active state of corrosion due to carbonation, they can vary between 1-10μA/cm^2 [24, 25, 21, 26, 22]. For chloride-contaminated concrete structures, current densities are significantly higher [17] and values of

10-25μA/cm^2 [27] up to 100μA/cm^2 [28, 29] are reported. In the case of impressed current techniques, an external current is applied to the specimens and the induced flow of electrons causes the corrosion of the steel. The current density used is therefore higher than that due to the natural electrochemical corrosion process. In the majority of the studies, high currents above 200μA/cm^2 led to increased transverse strains and greater crack widths [30, 31, 32, 7, 23, 33]. However, the results by Alonso et al [21] using currents between 3-100μA/cm^2 showed opposite trends. This could be explained by the combination of two factors: the varying nature of the corrosion products that develop over time, and the rate at which they diffuse in the concrete voids. For very low current densities corrosion products are allowed to develop naturally over longer periods, with enough time for oxygen to react with them. Thanks to oxygen availability, corrosion products are dryer and expand before diffusing in the voids. At higher current densities, conditions of limited oxygen cause the development of liquid corrosion products [34] that are free to flow through the voids. A gradual dissipation of corrosion product in the concrete porous structure occurs [35] and they solidify only when oxygen is available [36, 12], delaying and reducing expansions and crack growth. Moreover, the presence of chlorides, even at low concentrations, increases the iron solubility significantly, facilitating the flow of corrosion products and the development of non-uniform and localised pitting corrosion [37, 12]. For even higher current densities, the development of corrosion is so rapid that expansive pressures are generated before a diffusion of corrosion products can occur. As a consequence of the phenomena mentioned above, it follows that the same degree of corrosion can lead to different levels of expansion and cracking.

Some authors studied the process that leads to the onset of surface cracking to predict the so called time-to-cracking. This is outside the scope of the present work but a comprehensive review of the relevant literature is given by Jamali et al [13]. Among their conclusions it is worth noting the scatter in the available results and the lack of agreement between models, either experimental, analytical or numerical. They point out that increasing model complexity does not lead to more accurate estimations. They also emphasise that it is not sufficient to use the concept of a 'corrosion-accommodating region' (a porous zone between steel and concrete where corrosion products can accumulate before developing expansive pressures) as a fitting parameter to improve the accuracy of model predictions.

Other studies [38, 39, 40, 21, 7, 41, 42, 43, 44, 45, 3] focused on the correlation between surface crack width and level of internal corrosion, in the attempt to develop models that could be used as non-destructive assessment tools. Results from a few studies are summarised in Fig. 2.a, where significant scatter can be observed. Bossio et al [3] partially attribute the variability of predictive models to the influence of the relative position and distance between cracks, and the volumetric expansion coefficients of corrosion products that can vary significantly [13]. Zhao et al [44] observed that corrosion products distribute in the corrosion-accommodating region around the bar, and diffuse differently in the internal cracks and those that reach the outer concrete surface.

Other authors [5, 46, 39, 47, 6, 32, 48, 49, 18, 50, 16] studied the bond degradation as a function of the level of corrosion. Reviews of the relevant literature can be found elsewhere [17, 23]. Fig. 2.b shows the results of pull-out test from the literature, where the bond stresses are normalised with respect to reference uncorroded specimens. Despite the dispersion and variability that characterise the results, a common trend can be observed with an initial increase and a subsequent sharp decrease in bond strength. This change is typically associated with the development of surface splitting cracks.

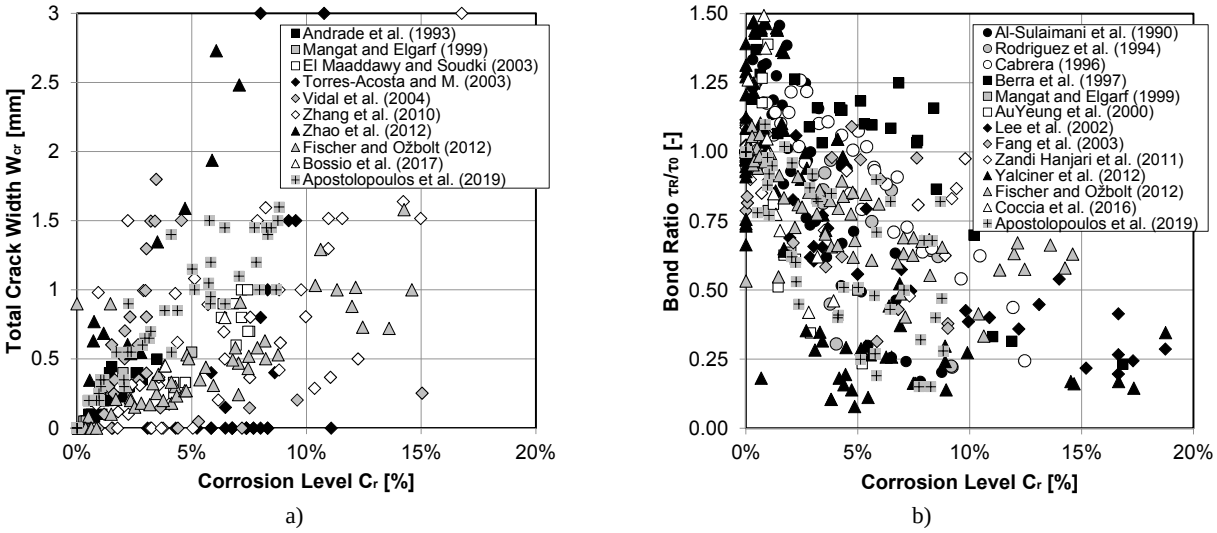

Figure 2: Comparison of experimental results from previous authors (data derived from plots where not explicitly presented in published work): (a) Crack width and corrosion [38, 48, 7, 41, 42, 43, 51, 44, 3, 52, 53]; (b) Bond deterioration and corrosion [5, 47, 39, 54, 48, 49, 55, 18, 50, 51, 56, 16, 52, 53].

From the perspective of the assessment of bond deterioration, any predictive approach based on the existing results would appear to be a two-step process: the measurement and analysis of surface crack widths leads to an estimation of the level of reinforcement corrosion, and this information is separately used as an input for another model to evaluate the subsequent loss of bond strength. It follows that the uncertainties associated with each step of the process contribute to an even greater overall inaccuracy.

An alternative approach is to use surface cracks as a direct measure of bond degradation, regardless of the corrosion level that caused them. This is based on the two following fundamental assumptions. Firstly, the load transfer through ribs interlock is predominant with respect to the frictional contribution after cracking. Secondly, a direct correlation between interlock reduction and crack width intrinsically disregards the uncertainty associated with localised corrosion, actual volumetric expansion coefficients, percentage of corrosion products that diffuse in the corrosion-accommodating region or flow into the cracks. In other words, surface crack width is a measure of the net effects of corrosion on bond, as conceptually shown in Fig. 3.

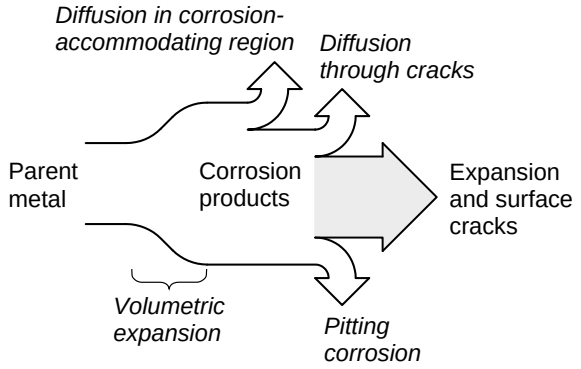

Figure 3: Conceptual diagram of surface cracks as an indicator of the net amount of corrosion products causing expansive effects (not to scale).

Table 1: Residual bond strength for corroded bars, after fib Model Code 2010 [62]

Conf.	Corrosion Penetration x [mm]	Equivalent Surface Crack w [mm]	Residual Capacity (Ratio to f_{bd}) [%] Ribbed	Plain
No Links	0.05	0.2-0.4	50-70	70-90
	0.10	0.4-0.8	40-50	50-60
	0.25	1.0-2.0	25-40	30-40
Links	0.05	0.2-0.4	95-100	95-100
	0.10	0.4-0.8	70-80	95-100
	0.25	1.0-2.0	60-75	95-100

Recent results have suggested that crack width is a potentially good indicator of bond deterioration, from either accelerated corrosion experiments [57, 58, 51, 59, 53] or tests on naturally corroded bridge girders [52]. Other authors [60, 61] have studied the influence of pre-existing splitting cracks on bond, independently from the presence of corrosion products. Among the common conclusions are the significant impact of longitudinal cracks on bond reduction and the importance of transverse confinement. The Model Code 2010 [62] also gives a simplified correlation between level of corrosion, crack width and bond degradation, summarised in Table 1. However, to the authors' knowledge, the flow of corrosion products was not identified as a key phenomenon in existing studies where crack width was suggested as an indicator of bond deterioration. In the present work, the flow of corrosion products is investigated as the primary cause for the lack of direct correlation between mass loss and bond. Mass losses due to corrosion are separated and decoupled from their expansive effects causing concrete cracking, using different sealing conditions on the specimens. The objective of the current work is to study a fundamental aspect of the bond behaviour and to justify a comprehensive theory that can underpin other studies, therefore moving from correlation to causality.

The objective of this publication is to investigate a new approach to the assessment of bond deterioration in reinforced concrete, based on surface crack width as the key damage indicator. Experiments were carried-out on un-

confined concrete cylinders with an embedded steel bar, and corrosion of the reinforcement was generated artificially using an impressed current. The sealing conditions varied between specimens to obtain similar levels of corrosion with different crack widths. The correlation between corrosion, cracks and reduction in bond strength was studied.

2. Experimental programme

A total of 60 cylindrical concrete specimens without transverse confining reinforcement were tested. The first part of the experimental programme consisted of accelerated corrosion testing using an impressed current. The pattern and width of corrosion-induced cracks was subsequently measured. The specimens were then subjected to concentric pull-out tests and the force-slip behaviour was measured.

An overview of the specimen series and numbering system is given in Table 2. The theoretical target mass losses were between 2.3-18.5% and the last Series was uncorroded and used as a reference. In the numbering system, the first letter (A to C) identifies the Series that were mixed and cast at the same time. The subsequent number corresponds to the nominal diameter of the steel bar, equal to 10 mm for all tests. The last two digits of each series indicate the theoretical percentage mass losses. For each value of target mass loss, five specimens (labelled *a* to *e*) were tested under the same conditions to provide a statistically significant distribution of the results.

Table 2: Test matrix

Series	Theoretical Mass Loss C_F	Corrosion time [days]
A10-17	17.3%	67.0
A10-08	8.0%	31.2
A10-05	5.4%	21.2
A10-02	2.3%	9.0
B10-10	10.2%	39.8
B10-07	7.4%	28.9
B10-05	5.4%	20.9
B10-04	3.8%	14.9
C10-19	18.5%	72.2
C10-12	12.1%	47.2
C10-08	7.8%	30.3
C10-00	0.0%	00.0

The specimens were submerged in a salt-water solution to diffuse and allow an even distribution of current [6]. In Series A, all sides of the cylinders were left exposed to the salt-water bath. In Series B and C, the bottom side of the cylinders was waterproofed with silicon sealant to avoid direct contact with the water. This allowed for a more homogeneously distributed current flow along the cylinders, without concentrations at the base of the specimen. Moreover, in Series C the unbonded length of the bar was covered with a 1 mm thick layer of paraffin, and the

interface between steel bar and concrete at the top side was also sealed to stop corrosion products from exuding out of the specimen. Expansive pressures and cracking are caused only by the fraction of corrosion products that are constrained inside the surrounding concrete. Similar levels of corrosion on specimens with different sealing conditions therefore allowed different amounts of corrosion products to diffuse and flow out. Similar levels of corrosion therefore induced different surface crack widths. The difference between Series is schematically shown in Fig. 4.

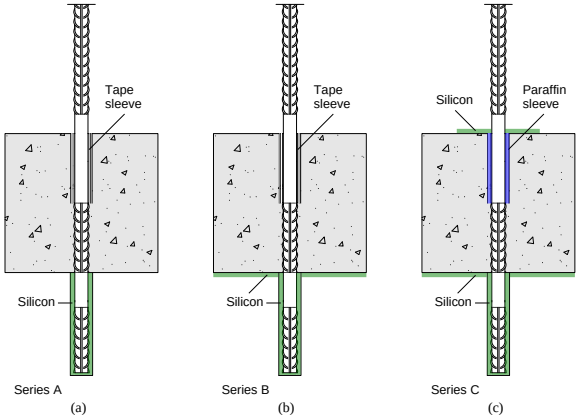

Figure 4: Difference in Series: (a) Series A with all concrete sides exposed and tape sleeve; (b) Series B with bottom face waterproofed with silicon sealant and tape sleeve; (c) Series C with silicon sealant on top and bottom faces and paraffin sleeve

2.1. Specimen geometry

The specimens were concrete cylinders with a diameter of 107 mm and a height of 100 mm. A ribbed steel bar with a nominal diameter $\varnothing = 10$ mm was cast concentrically in the cylinders. The nominal cover was $c = 48.5$ mm and the resulting cover-to-diameter ratio was 4.8. This value was adopted to obtain a pull-out failure by crushing of the concrete lugs in the uncorroded reference specimens, developing tensile hoop stresses in the concrete marginally lower than its tensile strength. One bar diameter was studied, to keep the same cover-to-diameter ratio for all Series without modifying the specimen dimensions and current intensity. This was deemed more important for this particular study than investigating other bar sizes. The dimensions of the specimen are not dissimilar to those recommended by RILEM [63] for concentric pull-out tests on cubic specimens. The bond length was $l_b = 5\varnothing = 50$ mm, based on RILEM [63] recommendations. This is considered a 'short' bond length where the bond stresses can be assumed constant along the embedded length. The geometry of the specimens is shown in Fig. 5.

A debonding sleeve was provided on the remaining 50 mm bar segment in the concrete and on the first outer 25 mm of the bar on the opposite side, measured from the concrete edge. In Series A and B, the sleeve was obtained by removing the ribs with a belt sander and wrapping the bar with layers of electrical and masking tape. In Series C, the debonding sleeve was obtained by applying a layer of paraffin of 1 mm thickness.

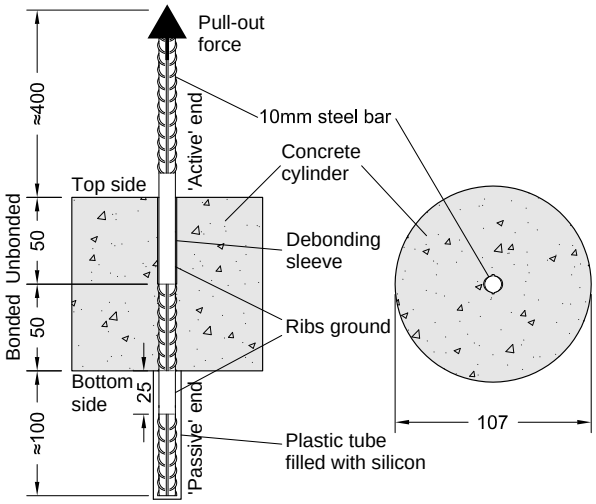

Figure 5: Specimen geometry: section along the longitudinal axis and transverse cross section through the concrete cylinder

The steel bar protrudes beyond the loaded face of the concrete cylinder by approximately 400 mm on the *active* side (in Fig. 5 this is shown as the top part where the tensile force was applied) to provide a sufficient length for the wedge grip of the testing machine and the measuring devices. The bar extends on the opposite *passive* side (beyond the unloaded face) of the cylinder by approximately 100 mm so that measuring devices can be installed on the unloaded end of the bar.

2.2. Materials

The specimens consisted of C25/30 concrete and high-strength steel bars. The composition and mechanical properties of the materials are hereby described.

2.2.1. Concrete

The concrete mix and the proportions of constituents are summarised in Table 3. The mix was chosen as an Ordinary Portland Cement (OPC) mix without any admixtures. The fine aggregate consisted of river sand and the coarse aggregate was uncrushed coarse gravel. It should be noted that the maximum aggregate size of the concrete was 10 mm.

At 28 days after casting, material characterisation tests were carried out in accordance with and EN 12390-3:2009 [64] and EN 12390-6:2009 [65] to obtain the control parameters: f_c, the compressive strength of concrete cylinder (dia: 100 mm, height: 200 mm); $f_{c,cub}$, the compressive strength of 100 mm concrete cubes and $f_{ct,sp}$, the split tensile strength of concrete cylinder (dia: 100 mm, height: 200 mm). The results for each Series of specimens are summarised in Table 4 based on three repetitions. The 28 day concrete cube strength results were similar across

Table 3: Concrete mix

Constituent	Type	Density $[kg/m^3]$	Amount $[kg/m^3]$
Water	-	1,000	180
Cement	CEM II-A-LL 32.5 R	3,100	300
Fine Aggregate	0/4 mm	2,625	835
Coarse Aggregate (uncrushed)	4/10 mm	2,625	1,015

all series and the average strength was 30.8 MPa. Series A exhibited lower compressive cylinder strength and split tensile strengths, whereas the highest strength values were obtained for Series B. On average, the split tensile strength was 2.8 MPa. The control tests were replicated at the time of the pull-out tests, that took place on average 88 days after casting. The concrete strength values were not significantly different at the time of the pull-out tests.

Table 4: Concrete properties at 28 days. Standard Deviation (SD) in brackets

Series	f_c [MPa]	$f_{c,cub}$ [MPa]	$f_{ct,sp}$ [MPa]
A	22.8 (0.92)	32.0 (0.89)	2.5 (0.18)
B	30.7 (0.66)	31.0 (2.46)	3.0 (0.40)
C	28.2 (0.83)	29.4 (0.65)	2.8 (0.18)

2.2.2. Steel reinforcement

The reinforcement bars were made of high-strength hot-rolled steel. The yield strength f_y = 530 MPa (SD= 1.23 MPa) and ultimate tensile strength f_u = 619 MPa (SD= 3.33 MPa) were obtained from uniaxial tensile tests, as the average values over four tests. The reinforcement bars have two longitudinal continuous ribs on opposite sides and two series of diagonal parallel ribs oriented at 48° with respect to the longitudinal axis. The maximum rib height was 0.75 mm.

The steel bars were previously stored in an uncontrolled environment and they developed a thin layer of surface rust. Before casting, all the steel bars were polished and the surface rust was removed mechanically with rotating metal brushes and an abrasive water-jet. Before and after being polished, the bars were weighed on an electronic scale with a capacity of 15.0kg and a resolution of 0.2g. On average, the rust corresponded to approximately 0.2% of the initial mass of the bars. Although the presence of a thin layer of rust before casting is common in real structures, the removal was important in the experiment because the test results should only reflect the degree of corrosion developed in the hardened concrete and responsible for confined expansive stresses.

Prior to removing the ribs along the debonded length, the bars were weighed and the results were related to the bar lengths. The calculated mean mass per unit length of the bars was g_0 = 611.6g/m with a Standard Deviation (SD)

of 1.8g/m. After the ribs were ground off along the unbonded length, the mass of the individual bars was recorded.

Authors [66, 67, 68, 69] have concluded that the orientation of the bar during casting with respect to the direction of gravity has an influence on the characteristics of the 'interfacial transition zone' between the concrete and steel, and the concrete on bottom side of a bar is more porous than elsewhere. Voids in this porous zone would delay the cracking onset. This effect was not replicated in the experiments, as the cylinders are cast and cured with the main axis in the vertical position, as will be described in the subsequent section.

2.3. Mixing, casting and curing

Fresh concrete was mixed using a mixer with a capacity of 100 litres. Polyvinyl chloride (PVC) pipes with an inner diameter of 107 mm were used as moulds for the cylinders. The moulds and reinforcing bars were held in position with a timber frame during casting. The longitudinal axis was oriented vertically with the bonded length on the upper part of the cylinders. The specimens were cast and compacted on a vibrating table in 2 layers, and immediately covered with plastic sheets. Approximately 24 h after casting, the specimens were removed from the timber frame, wrapped in plastic sheets (while kept inside the plastic moulds) and left to cure in an indoor environment. The curing conditions were uncontrolled.

After a standard curing period of 28 days, the plastic sheets and moulds were removed. To avoid direct contact between the steel bars and the chloride-rich water of the accelerated corrosion tests, the shorter protruding bar ends were protected in plastic tubes and sealed with silicon. As mentioned previously, in Series A the bottom face of the concrete cylinders was not sealed. In Series B and C, the bottom face of the cylinders was waterproofed with silicon sealant to avoid direct contact with water and allow a more uniformly distributed current flow along the cylinders, without concentrations at the base of the specimen. In Series C, the top face was also sealed.

2.4. Accelerated corrosion

A current density of 200μA/cm^2 was used in the experiments, in line with the recommendation that current densities lower than 200-250μA/cm^2 are most appropriate for accelerated laboratory testing [31, 7, 23]. As described in the Introduction, other authors [30, 31, 32, 7, 23, 33] have indicated that higher currents lead to increased expansions that are not representative of the effects of corrosion in structures that are in service. Faraday's law of electrolysis [7, 23], shown in Equation 2, was used to calculate the approximate time required to develop different levels of corrosion:

$$\Delta m_F = \frac{I \cdot t \cdot M}{F \cdot z} = \frac{I \cdot t \cdot 55.845}{96,487 \cdot 2} \tag{2}$$

where Δm_F is the theoretical mass loss [g], I is the current intensity [A], t is time [s], M is atomic weight of metal (55.845g/mol for Fe), F is Faraday's constant (96,487 C/mol) and z is the ionic charge.

The specimens were submerged in a 5% Sodium Chloride (NaCl) water solution in separate plastic boxes for at least 3 days before current was impressed to generate corrosion. Stainless steel plates were used as cathodes. During the experiments, the boxes were closed with a plastic lid to avoid evaporation and therefore changes in the NaCl concentrations. The shorter protruding bar ends at the bottom of the cylinders were protected in plastic tubes and sealed with silicon. This was necessary to avoid direct contact between the steel bars and the chloride-rich water of the accelerated corrosion tests. The set-up is shown in Fig. 6.

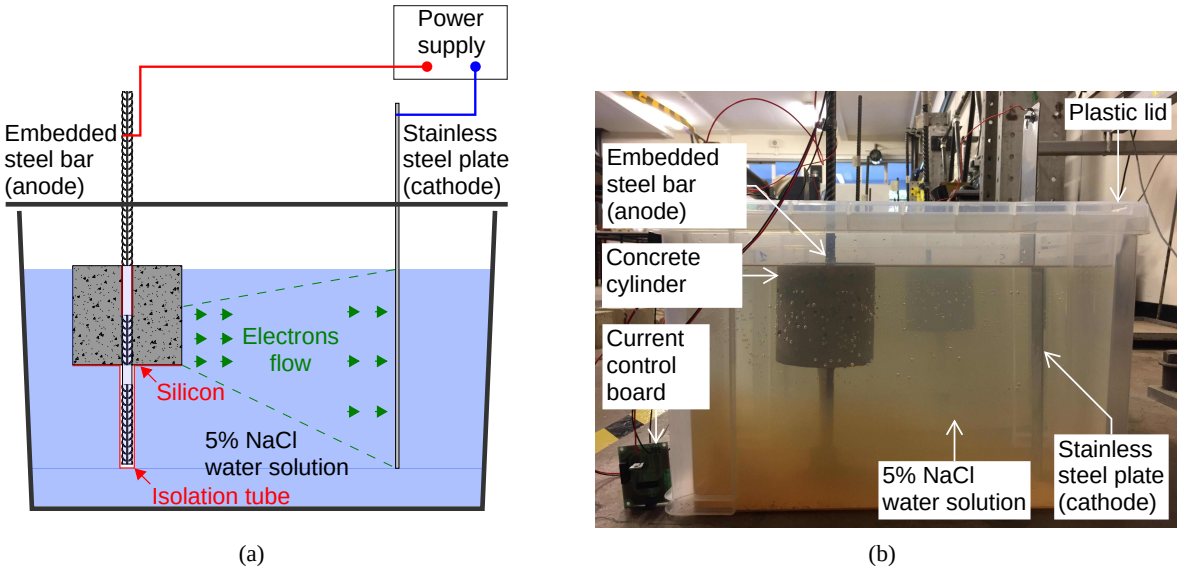

Figure 6: Set-up of accelerated corrosion testing. (a) Schematic; (b) Photograph of laboratory experiment

Specimens with the same target corrosion levels were connected in series, to ensure that the same current was impressed. The different series, each corresponding to a given target mass loss, were connected in parallel. Power supplies with a maximum voltage of 32 V were used. Current control boards were developed to control the current intensity with an accuracy of ±1%.

The different series had to be kept under impressed current for different periods of time. Corrosion was therefore initiated on a different day for each series, but the tests were stopped on approximately the same day. Subsequently, the specimens were removed from the salt-water bath and allowed to dry. The corrosion products solidified in the presence of oxygen, during the period between the removal from the salt-water bath and the pull-out tests that was consistent across all series. This was desirable so that the concrete was of the same age (therefore approximately the same strength) for all the series at the end of the accelerated corrosion testing, and the drying period before pull-out

testing was also approximately the same. This allowed for more reliable and consistent bond strength results.

2.5. Crack width measurement

At the calculated time the impressed current was interrupted, the specimens were removed from the salt-water bath and left to dry for at least one day. Surface crack widths were measured using an optical microscope with a magnification factor of 40X. The divisions of the ocular scale were of 0.02 mm and the accuracy of the measurements can be assumed to be half the division size, therefore 0.01 mm. Where multiple cracks developed, the total number of cracks and the angles between them on a plane orthogonal to the longitudinal axis were recorded. In the case of multiple cracks, the total crack width W_{cr} was used for the analysis of the results, calculated as the sum of all crack width values along a directrix (a circumferential line at a given longitudinal coordinate ξ). The definition of total crack width is indicated in Eq. 3.

$$W_{cr} = \max\Big(\sum_{i=1}^{n} w_i\Big)_{\xi} \tag{3}$$

The use of a cumulative value, rather than the width of a main crack, has been used by other authors [70, 71, 57] and acknowledged as a meaningful parameter. The reference system used is shown in Fig. 7. As the crack widths were not uniform along the cylinders, only the maximum crack width values were used in the analysis of the results.

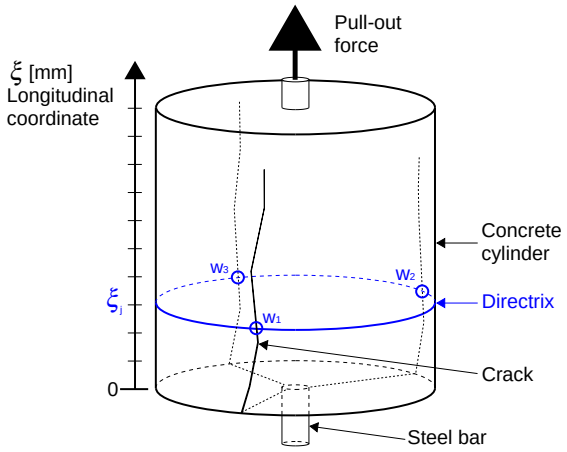

Figure 7: Total crack width at a given coordinate

2.6. Pull-out tests

After the period of accelerated corrosion had been completed, concentric bond pull-out tests were carried out on the corroded specimens using a universal testing machine with a load capacity of 150 kN. A photo of the testing set-up is shown in Fig. 8. A horizontal steel plate with a central hole and longitudinal stiffeners was used as a reaction

frame. The plate was bolted to the base of the Instron machine with four Grade 8.8 M10 Holding Down (HD) bolts. The tensile force was applied vertically on the bar using a grip wedge clamp. The tests were carried in displacement control. Tests on Series A and C were conducted at a rate of 2.4 mm/min. For Series B, the rate was reduced to 1.2 mm/min to better capture the post-peak softening branch of the load-slip curve. Two Linear Potentiometric Displacement Transducers (LPDTs) were clamped to the bar on the passive side of the specimen, to measure the slip between the bar and the bottom flat face of the concrete cylinder. Two additional transducers were clamped to the active side of the reinforcing bar. They effectively measured the relative displacement between the cross section of the bar at the centre of the clamp and the top of the steel plate. A nominal elastic correction is to be applied in the analysis of the results, to take into account the elongation of the steel bar between the points of measurement. Data from the transducers on the active side was used to cross-check that from the passive side transducers.

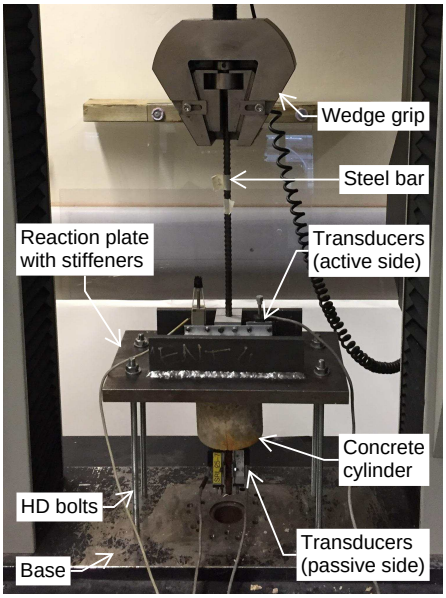

Figure 8: Photo of concentric pull-out test set-up

2.7. Rust removal

At the end of the pull-out tests, the concrete cylinders were broken open and the steel bars removed and cleaned. The corrosion products were removed by partially submerging the bars in a 11% solution of Hydrochloric Acid (HCl) for approximately 18 h and gently scrubbed with a metal brush. After the rust was removed, the bars were weighed and the final mass m compared with the initial mass m_0 measured before the accelerated corrosion tests. The mass loss was calculated as the difference between the two values.

3. Results

The experimental results are presented here in terms of measured average mass loss, attack penetration, total surface crack width, ultimate bond strength, ultimate bond strength ratio and failure mode. A summary is given in Table 5. The results are grouped by Series, each value therefore represents the average of five specimens tested under the same conditions. No adjustment was made on the results to take into account any difference in concrete strength from material characterisation tests.

Table 5: Summary of results for each Series: measured average mass loss, calculated attack penetration, total surface crack width, ultimate bond strength, ultimate bond strength ratio. Results are average values, calculated over five specimens tested under the same conditions.

Series	Measured mass loss C_r [%]	Attack penetration x [mm]	Number of cracks [-]	Total crack width W_{cr} [mm]	Ultimate bond strength τ_R [MPa]	Bond strength ratio τ_R/τ_0 [-]	Pitting corrosion
A10-17	24.3%	0.65	-	-	19.8	1.22	Severe
A10-08	10.3%	0.27	-	-	20.6	1.27	Moderate
A10-05 *	16.9%	0.44	2.4	0.97	10.1	0.63	Moderate
A10-02	5.1%	0.13	-	-	19.6	1.21	Mild
B10-10	10.2%	0.26	2.4	0.36	16.4	1.01	No
B10-07	8.5%	0.22	2.0	0.19	16.4	1.01	Moderate
B10-05	6.7%	0.18	1.2	0.08	17.9	1.11	Moderate
B10-04	5.1%	0.13	-	-	17.3	1.07	Mild
C10-19	22.9%	0.61	1.6	0.20	15.4	0.95	Severe
C10-12	16.7%	0.44	2.0	0.10	16.1	0.99	Moderate
C10-08	11.2%	0.29	1.6	0.19	14.4	0.89	Mild
C10-00 (reference)	0.0%	0.00	-	-	16.2	1.00	-

* malfunction led to $i_{corr} > 200\mu A/cm^2$

Where present, the number of cracks on each cylinder varied, ranging from 1 to 3. The average number of cracks over five specimens corroded under the same conditions is reported in Table 5. For the reference uncorroded specimens, the peak bond strength was equal on average to 16.2 MPa (SD= 0.71 MPa). The ultimate bond strength for each Series was also normalised with respect to that of the reference specimens for a better interpretation of the results, and expressed as a bond strength ratio. It can be noted that in all Series where cracks in the concrete were not present or did not reach the outer surface, the bond strength ratio was higher than unity. Severe pitting corrosion was observed in some samples. This effect is also reported in the table, based on visual observations of the maximum pit depth, extent of localisation along the longitudinal axis and variation among bars of the same Series. In the classification, *Mild* can be related to maximum pit depths of approximately 1.0-2.0 mm, *Moderate* to 1.5-2.5mm and *Severe* to 2.0-3.0 mm.

Due to a malfunction of one control board, Series A10-05 was subjected to a higher level of current density. This led to much higher corrosion than predicted. Based on the comparison between measured mass loss and prediction

based on Faraday's law, it is plausible that the actual current density impressed on Series A10-05 was between 320 – 580$\mu A/cm^2$. The mass loss of specimen B10-05b was not recorded.

3.1. Gravimetric measurements

The experimental mass loss Δm was calculated as the difference in bar weight before and after the accelerated corrosion tests:

$$\Delta m = m_0 - m \tag{4}$$

It was assumed that the mass loss occurred homogeneously along the bonded length of the bar $l_b = 50$ mm. The mass loss can be expressed as a percentage of the initial mass, based on the measured average weight per unit length of the bars g_0:

$$C_r = \frac{\Delta m}{g_0 \cdot l_b} \cdot 100\% \tag{5}$$

Under the assumption of homogeneous distribution, the level of corrosion is also expressed as the average attack penetration (or penetration depth) x, calculated as follows:

$$x = \frac{\varnothing}{2} \cdot \left(1 - \sqrt{1 - C_r}\right) \tag{6}$$

This parameter effectively corresponds to a reduction in radius of the steel bar.

3.2. Surface crack widths

Specimens in Series A (A10-02, A10-07, A10-15) reached significant levels of corrosion up to 25.5% without developing visible surface cracks, with the exception of A10-05. Specimens in Series B and C exhibited corrosion-induced surface cracking.

As an example of the evolution of the crack width with cylinder height, the total crack width measurements for specimens B10-10e ($C_r = 10.5\%$), B10-07e ($C_r = 7.8\%$) and B10-05e ($C_r = 5.9\%$) are shown in Fig. 9. The plot shows that the crack width varied with height and was not uniform. The maximum value typically occurred at the bottom of the cylinders, although not in all cases. Therefore, the retained value did not always correspond to the same longitudinal coordinate along the height of the cylinder.

The results expressed as the maximum total crack width versus corrosion level are shown in Fig. 10. The square markers represent results from Series A, where the bottom concrete face was not sealed. The squares marked with a

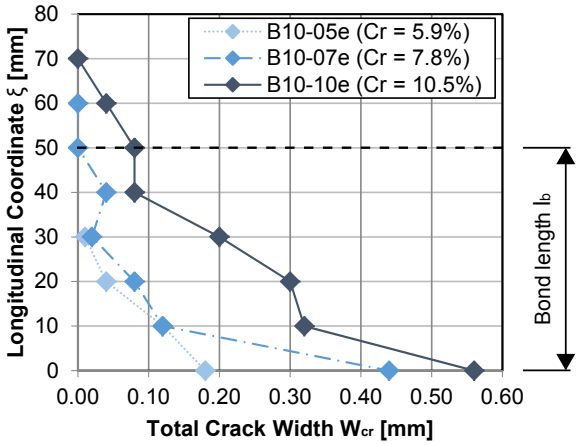

Figure 9: Example of total crack width evolution along the cylinder height for three representative specimens. The horizontal dashed line indicates the end of the bonded length.

'X' denote Series A10-05, where a current density higher than $200\mu A/cm^2$ was impressed. The rhomboidal markers indicate the results from Series B, where the bottom face of the specimens was sealed with silicon, whereas triangular markers denote Series C with both the top and bottom faces sealed. The continuous line is a linear regression of all results.

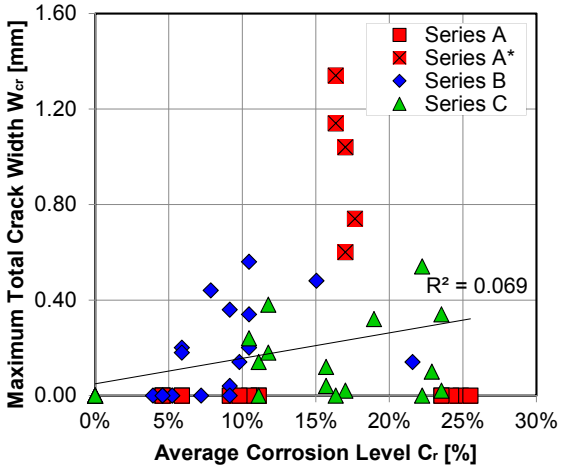

Figure 10: Correlation between average corrosion level and maximum total crack width (* denotes tests where malfunction led to $i_{corr} > 200\mu A/cm^2$).

It is evident that none of the specimens in Series A subjected to the correct current density exhibited surface cracking. In specimens where surface cracks were present, the onset of cracking appeared to correspond to mass losses of approximately 5.0%. However, as indicated previously, several specimens did not exhibit any cracking even after significant mass losses higher than the above mentioned threshold.

3.3. Bond stress-slip behaviour

Nominal bond stresses τ were calculated assuming a uniform stress distribution along the bond length. The ultimate bond strength τ_R is defined as the peak value under the maximum tensile force:

$$\tau_R = \frac{F_u}{\pi \cdot \varnothing \cdot l_b} \tag{7}$$

where the bond length $l_b(s)$, initially equal to 50 mm, is reduced as the slip s increases during the test:

$$l_b(s) = l_{b,0} - s \tag{8}$$

The slip was calculated as the mean value from the two transducers on the passive side. In one specimen (B10-07a) premature failure occurred by rupture of the steel bar in tension, probably due to pitting corrosion and a localised reduction in cross section of the bar. In all the other tests the bond stress-slip curves were characterised by an initial elastic behaviour of linear proportionality, a decrease in stiffness due to the development of internal cracking. After the ultimate peak strength was reached, specimens that failed by pull-out exhibited a post-peak softening branch and a gradual reduction in strength with increasing slip. Pull-out failures occurred by crushing or shearing of the concrete lugs under the steel ribs as hoop stresses in the concrete remained below its tensile strength. Specimens that failed by splitting exhibited a drop in bond strength and a sudden increase in slip due to the development of macro-cracks. Expansive pressures from corrosion products had already induced tensile hoop stresses in the concrete, which exceeded the concrete strength during pull-out testing, leading to the development of splitting cracks. The tests were stopped when the slip reached 20 mm, except for Series A10-02 where the tests were interrupted at smaller slip values due to an error in the loading protocol. The average bond stress-slip results of the pull-out tests for each series are described in the following sections.

3.3.1. Uncorroded Specimens – Reference

A representative plot of the average bond stress versus slip for one of the uncorroded reference specimens of Series C10-00 is shown in Fig. 11.a (C10-00b), where the grey area represents the domain between the maximum and minimum experimental curves among the five repetitions. The majority of the specimens failed by pull-out and only one splitting failure occurred (C10-00e), validating the test design on the development of hoop stresses just below the concrete tensile strength. The peak bond strength ranged between 15.5 and 17.2 MPa with an average of 16.2 MPa. This mean value was used to subsequently calculate bond strength ratios.

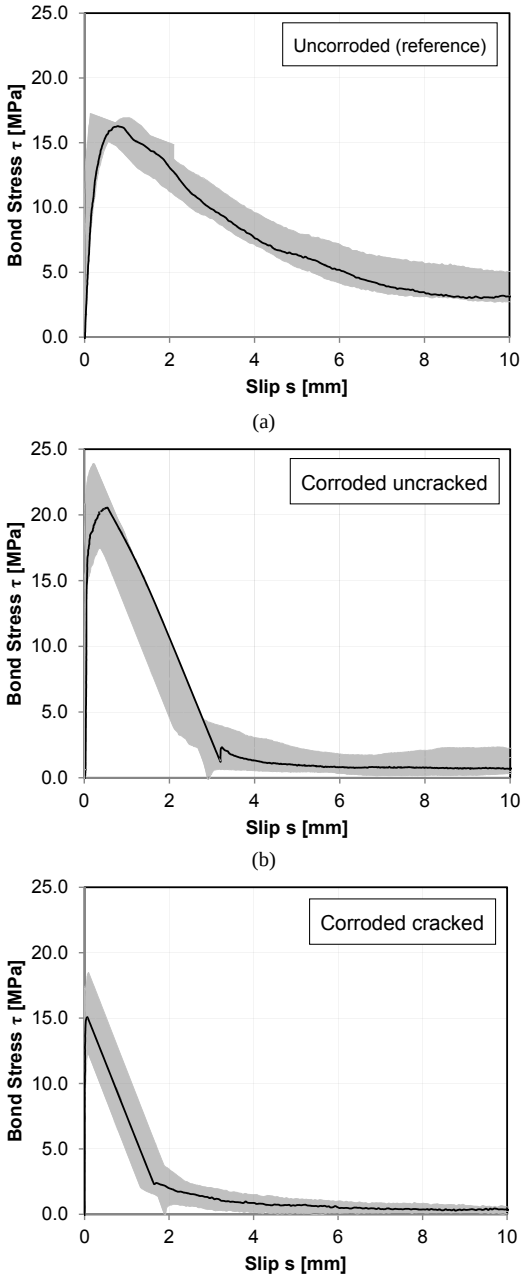

Figure 11: Bond stress-slip plots: (a) C10-00b (C_r = 0.0%) and Series C10-00; (b) A10-08d (C_r = 10.5%, uncracked) and Series A10-08; (c) C10-19c (C_r = 22.9%, cracked) and Series C10-19. Maximum and minimum curves within each Series shown in grey

3.3.2. Corroded specimens – Uncracked prior to bond pull-out testing

For Series A10-02, A10-08, A10-17, B10-04 the corrosion-induced expansive stresses did not attain the critical value that would cause longitudinal cracks to fully develop and reach the concrete surface. During pull-out testing both splitting and pull-out failure modes occurred, although most of the specimens (73%) exhibited splitting failures. As a representative example, the test results for specimen A10-08d (C_r= 10.5%) are shown in Fig. 11.b. It can be observed that the presence of corrosion induced an increase in initial stiffness and a reduction in slip corresponding to the peak stresses. The ultimate bond strength is on average higher than the reference value. The plot also shows that splitting of the concrete led to a brittle failure, a significant drop in stresses after the ultimate strength is reached and a sudden increase in slip.

3.3.3. Corroded specimens – Cracked prior to bond pull-out testing

In the cases where corrosion-induced cracking reached the concrete surface prior to pull-out testing (Series A10-05, B10-10, B10-07, B10-05, C10-19, C10-12, C10-08), the majority (84%) of specimens failed by splitting, which mostly occurred by further opening of existing corrosion-induced cracks. The test results for specimen C10-19c (C_r= 22.9%) are shown in Fig. 11.c, as a representative case of the behaviour of specimens that exhibited corrosion-induced cracking. It can be seen that peak stresses are lower than those of uncracked specimens, although the failure mode by splitting led to a similar stress-slip curve.

3.4. Ultimate bond strength and corrosion level

The ultimate bond strength ratio, calculated with respect to the mean strength of 16.2 MPa of the reference uncorroded specimens, is plotted versus the degree of corrosion in Fig. 12.b, irrespective of the failure mode. The relationship between bond strength versus the level of corrosion differs from the findings of previous authors, shown in Fig. 2.b. The plot does not show a significant reduction in ultimate bond strength, even beyond the supposed cracking point. Significant mass losses are obtained with limited reduction in bond strength. The same results are plotted in terms of ultimate bond strength ratio versus maximum total crack width in Fig. 12b. Series A10-05 exhibited the greatest bond strength reduction, where a current density higher than $200\mu A/cm^2$ was impressed (squares marked with 'X' in Fig. 12). This effect is in line with findings of authors [7] that with higher current densities have observed increased side strains, measured on the concrete surface in the transverse direction, therefore across the splitting cracks induced by corrosion of the reinforcement.

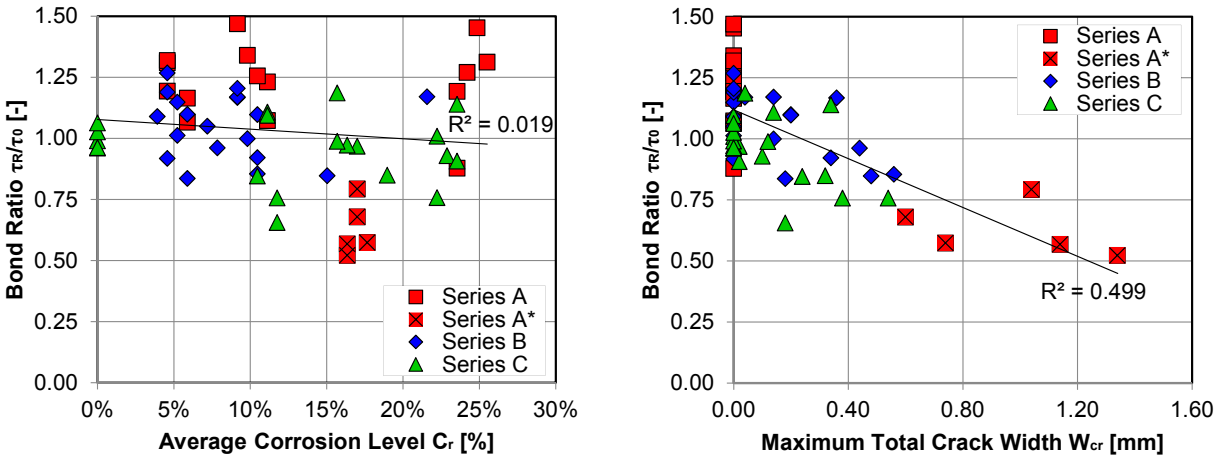

Figure 12: Correlation between ultimate bond strength and: (a) Mass loss; (b) Total crack width (* denotes tests where malfunction led to $i_{corr} > 200\mu A/cm^2$).

4. Discussion

It can be seen that significant scatter characterises the bond test results and no correlation can be found between average mass loss and bond strength ratio in Fig. 12.a. The results were also analysed using the attack penetration as measure of corrosion level. Similarly to Fig. 12.a, no correlation was found, leading to analogous conclusions. However, by using the total crack width as a damage indicator (Fig. 12.b), the scatter of the uncracked specimens is reduced as the associated data points 'collapse' to the left-hand side of the plot. The majority of uncracked specimens did not exhibit a reduction in bond strength, and any increase can be disregarded from an assessment perspective. A trend of bond deterioration with increasing crack width can be observed, where the ultimate bond strength appears to reduce almost linearly. This is attributed to the fact that surface cracks indicate the net amount of corrosion products that caused expansion and reduction in rib interlock. The uncertainty related to the the fraction of corrosion products that do not cause expansions is therefore removed from the results. As indicated in the Results section, few specimens from Series A (those corresponding to Series A10-05) were subjected to a higher current, which possibly led to increased expansions. In Fig. 10 and Fig. 12.b it can be observed that Series A10-05 led to the greatest crack widths. Care should therefore be taken when interpreting those results. If those five data points are removed from the analysis, a correlation factor of $R^2 = 0.275$ is obtained. Even if the accidental data series are removed from the analysis, the bond strength results still show a better correlation with total crack widths, rather than mass loss or attack penetration. The authors believe that the dependence on the current density is reduced when using crack width as a bond deterioration indicator. In other words, the authors believe that what affects the analysis is the net expansion effect for the concrete, not the amount of corrosion products that caused it. Fig. 13 shows the correlation between surface crack width and

bond strength ratio, comparing the results of the current study with data from previous authors. Concerning the results from the present study, the scatter was discussed with respect to Fig 12.b, showing the same data. It can be observed that a trend exists and that the experimental results align well with those in the literature, despite the tests of the present study were designed to decouple corrosion from crack widths. The recommendation from Model Code 2010 [62] are in line with the experimental trends. Overall, they are conservatively on the lower part of the distribution.

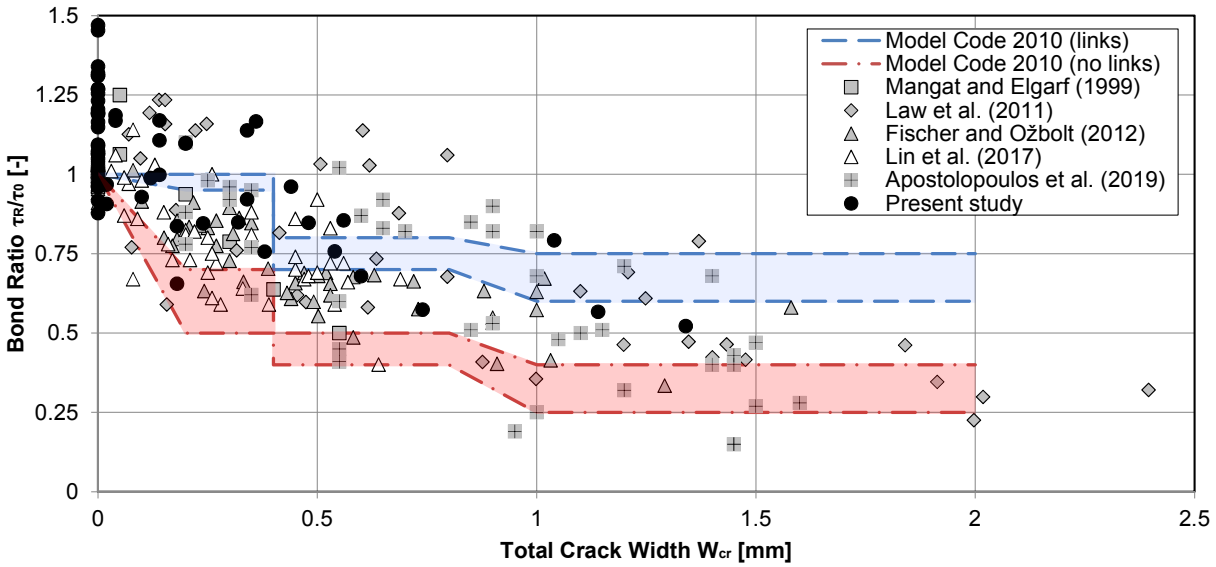

Figure 13: Correlation between ultimate bond strength ratio and surface crack width. Comparison between recommendations from Model Code 2010 [62], results from previous authors [48, 58, 51, 59, 52, 53] (data derived from plots where not explicitly presented in published work) and results from present study

It is reasonable to assume that a local relationship exists between equivalent bond stresses and the total crack width along the bar. The average bond stress ratios can therefore be compared with the mean total crack widths, as shown in the plots of Fig. 14.

It can be observed that the results expressed with respect to the mean value of the Total Crack Width along the bars do not yield a better correlation than those relative to the Maximum Total Crack Width previously shown in Fig. 10 and Fig. 12.b. Law et al [58] have carried out accelerated corrosion tests using an impressed current and eccentric bond tests. They observed that the maximum crack width led to a better correlation with bond strength than the mean crack width.

Leakage of part of the liquid corrosion products is considered to be the prime reason for not developing significant expansive pressures and subsequent cracking in the majority of specimens from Series A, where the bottom face was not sealed. This phenomenon was also observed in Series B, although to a lesser extent as the specimens were partially sealed. The greatest crack widths and bond reductions were expected in Series C due to the fully sealed conditions. However, Series B and C exhibited similar results. It is believed that the lack of oxygen in the specimens

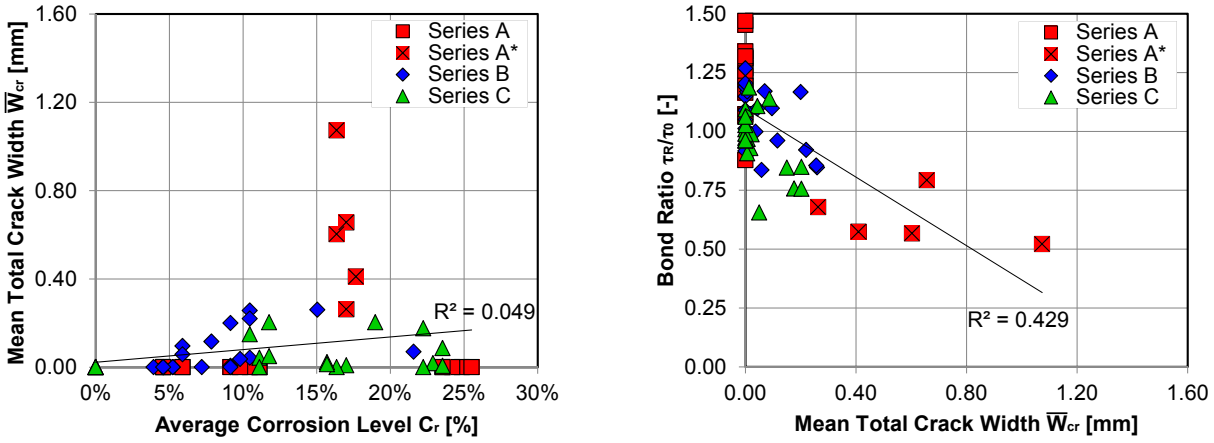

Figure 14: Correlation between mean total crack width and: (a) Average corrosion level; (b) Ultimate bond strength ratio (* denotes tests where malfunction led to $i_{corr} > 200\mu A/cm^2$).

prevented the precipitation of corrosion products and their expansive effects. In other words, sealing specimens has two opposing effects: corrosion products are locked inside the specimens, forcing expansive pressures. However, reducing the oxygen availability induces flow of liquid corrosion products and relieves expansive pressures. This possibly explains the lack of agreement in the experimental data available in the literature. It was not possible to directly compare results from other authors, as the characteristics of the debonding sleeves and seals are often not included in the published work. The results highlight the need for the development of a standardised accelerated corrosion methodology for bond tests. In laboratory experiments, the characteristics of the debonding sleeves and seals at their ends have an impact on the results. They therefore need to be considered in the test design. Fischer and Ožbolt [51] also acknowledge that only part of the corrosion products generate expansive pressures, and that such phenomenon is the reason for the difficulty in comparing results by other authors. This confirms that correlating corrosion level to bond degradation is difficult, since the proportion of corrosion causing expansion is unknown. Coccia et al [16] also point out that even for significant levels of corrosion, visible cracks do not always appear. They attribute this effect to the properties of the concrete matrix and mainly porosity. Other authors [72, 73, 14] used alternative cycles of wet and dry conditions during accelerated corrosion testing to allow the interaction of corrosion products and oxygen.

It is possible that with higher corrosion rates, expansive pressures are developed before the corrosion product are able to flow in the concrete inner structure. This effect could justify the behaviour of Series A10-05, where a higher current density was impressed and surface cracks developed.

The exposure to corrosion is not homogeneously distributed along the bonded length. This can lead to the devel-

opment of non-uniform corrosion around the bar. This effect was observed in several specimens, especially those of Series A where the bottom face was not sealed. The level of corrosion on the bottom portion of the bars was higher than the top. In Series B and C, where the bottom face was sealed and the distribution of current density was more homogeneous along the bar, localised corrosion at the bottom was significantly reduced. In some cases, severe pitting occurred at the top of the cylinders, where corrosion products exuded from the sleeve and stagnated on the flat concrete surface before precipitation. A local reduction in diameter of up to 30% of the original value was measured in extreme cases, such as in specimen B10-04a. The presence of localised corrosion undermines the validity of average mass loss values. If the mass loss is localised, the average mass loss over the bonded length is less than the calculated value. Moreover, corrosion was slightly more pronounced on one side of the bars. This was attributed to the position of the cathode, where one side of the specimen was more directly exposed to the current flow.

The measured values of mass loss are in many cases higher than the predictions based on Faraday's law. This phenomenon has been observed by other researchers [21, 15]. As described by Alonso et al [21], this can be partially explained by the spalling of the steel, where portions of uncorroded metal are detached due to the oxidisation of the surrounding material. Fig. 15 shows a local reduction in diameter that appears to be due to this effect.

Figure 15: Spalling of corroded steel on specimen A10-15a

The expansive stresses due to corrosion are only generated along the bonded length of the reinforcement bar. An unbonded concrete region is often necessary in specimens subjected to concentric pull-out bond tests, as it avoids parasitic confining effects from the reaction plate [74], and allows the development of inclined compression cones [75]. However, during the corrosion process this adjacent concrete region does not build up expansive stresses to the same extent. It effectively provides a confining action, reducing strains and bridging cracks in the top portion of the concrete cylinder as indicated schematically in Fig. 16. The maximum crack widths are in fact measured at the bottom of the specimens and reduce towards the top, as previously shown in Fig. 9. This represents a limitation of the bond test set-ups intended to capture both corrosion-induced cracking and bond deterioration. This consideration can be added to the objections previously raised [5, 74] on the use of concentric pull-out specimens. In future test specifications, debonding sleeves may be minimised in length and placed symmetrically to provide a more consistent framework to identify corrosion effects.

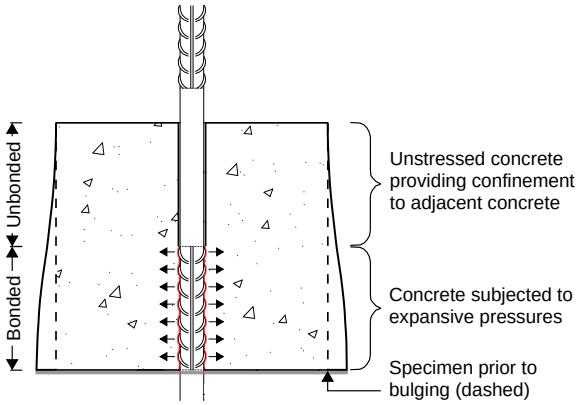

Figure 16: Confining effect provided by unstressed concrete along unbonded length. Indicative elastic deformations under expansive pressures (not to scale)

5. Conclusions

Concrete specimens with an embedded steel bar were subjected to accelerated corrosion using an impressed current. By changing the sealing conditions of the specimens, the amount of corrosion products able to flow through the concrete voids varied. With this new methodology, the level of reinforcement corrosion was separated and decoupled from its expansive effects that cause cracking of the concrete cover. Crack widths were measured on the concrete surface and concentric bond tests were subsequently performed on the specimens. The direct correlation between crack widths and bond strength deterioration was investigated. The results of this study and a critical analysis of the relevant literature lead to an improved understanding of the corrosion-induced bond degradation phenomenon. The findings of this study can contribute to the future development of a new and potentially more accurate approach for the structural assessment of deteriorated reinforced concrete structures. Improved and more accurate assessments can reduce the maintenance costs of the infrastructure network by limiting onerous interventions such as repairs, strengthening or replacement of entire bridges. The following conclusions are drawn from this study:

1. This study suggests that corrosion of the internal steel reinforcement and bond degradation may be only indirectly correlated. Concrete crack widths are potentially better indicators than corrosion level to characterise bond strength degradation of steel reinforcement. They can be interpreted as a measure of the net amount of corrosion products that generate expansive effects and a reduction in bar ribs interlock. Since these conclusions are limited to the type of specimen and testing conditions used in this study, more research is necessary to investigate the influence of the parameters involved (e.g. cover, bar size, cover/diameter ratio, confinement, concrete quality) to develop predictive models of general applicability.
2. In some circumstances, measures of corrosion such as mass loss or attack penetration are not suitable indicators of bond deterioration. In the present study, significant general corrosion (up to average mass losses of 25.5%)

occurred with limited reduction in bond strength when expansive pressures did not build up.

3. Conditions of limited oxygen and the presence of chlorides can lead to the development of liquid corrosion products. Before solidifying, they can flow in the voids and porous structure of the concrete. Expansive pressures are therefore relieved. As a result, corrosion-induced cracking can be delayed or not occur.
4. Accelerated corrosion using an impressed current in the presence of chlorides can lead to non-uniform corrosion along the bar and localised pitting corrosion.
5. The geometry and configuration of the specimens have an influence on the cracking pattern. A specimen design that follows recommendations for concentric pull-out bond tests presents challenges if corrosion-induced cracking is also studied: the presence of a debonding sleeve induces a stress-free concrete zone adjacent to the corroded part, which reduces corrosion-induced crack widths.
6. It is necessary to develop specifications and standardise accelerated corrosion testing methodologies for bond tests, with respect to both mechanical and chemical phenomena.

Acknowledgements

The authors wish to express their gratitude to the technical staff of the University of Cambridge Structures Research Laboratory for their contribution to the experimental work presented in this publication. The first author gratefully acknowledges the financial support of the United Kingdom Engineering and Physical Sciences Research Council (EPSRC) via a Doctoral Training Partnership [Grants RG75686, RG80792].

Additional data related to this publication are available at the University of Cambridge institutional data repository [76].

References

[1] I. Balafas, C. Burgoyne, Modeling the structural effects of rust in concrete cover, J. Eng. Mech. ASCE 137 (3) (2011) 175–185. doi:https://doi.org/10.1061/(ASCE)EM.1943-7889.0000215.

[2] M. Davis, N. Hoult, A. Scott, Distributed strain sensing to determine the impact of corrosion on bond performance in reinforced concrete, Construction and Building Materials 114 (2016) 481–491. doi:https://doi.org/10.1016/j.conbuildmat.2016.03.205.

[3] A. Bossio, G. Lignola, F. Fabbrocino, T. Monetta, A. Prota, F. Bellucci, G. Manfredi, Nondestructive assessment of corrosion of reinforcing bars through surface concrete cracks, Structural Concrete 18 (2017) 104–117. doi:https://doi.org/10.1002/suco.201600034.

[4] ASCE, Infrastructure Report Card, 2017, Tech. rep., American Society of Civil Engineers (2017).

[5] G. Al-Sulaimani, M. Kaleemullah, I. Basunbul, Rasheeduzzafar, Influence of corrosion and cracking on bond behavior and strength of reinforced concrete, ACI Structural Journal 87 (2) (1990) 220–231. doi:https://doi.org/10.14359/2732.

[6] A. Almusallam, A. Al-Gahtani, A. Aziz, Rasheeduzzafar, Effects of reinforcement corrosion on bond strength, Construction and Building Materials 10 (2) (1996) 123–129. doi:https://doi.org/10.1016/0950-0618(95)00077-1.

[7] T. A. El Maaddawy, K. Soudki, Effectiveness of impressed current technique to simulate corrosion of steel reinforcement in concrete, ASCE Journal of Materials in Civil Engineering 15 (1) (2003) 41–47. doi:https://doi.org/10.1061/(ASCE)0899-1561(2003)15:1(41).

[8] K. Bhargava, A. Ghosh, Y. Mori, S. Ramanujam, A proposed model for corrosion-induced bond degradation in reinforced concrete, in: F. A. Charney, D. E. Grierson, M. Hoit (Eds.), 17th Analysis and Computation Specialty Conference – Proceedings. 18-21 May 2006, American Society of Civil Engineers (ASCE), St. Louis, Missouri, USA, 2006, pp. 302–316. doi:https://doi.org/10.1061/40878(202)24.

[9] K. Bhargava, A. Ghosh, Y. Mori, S. Ramanujam, Corrosion-induced bond strength degradation in reinforced concreteanalytical and empirical models, Nuclear Engineering and Design 237 (11) (2007) 1140–1157. doi:https://doi.org/10.1016/j.nucengdes.2007.01.010.

[10] Y. Yuan, Y. Ji, S. Shah, Comparison of two accelerated corrosion techniques for concrete structures, ACI Structural Journal 104 (3) (2007) 344–347. doi:https://doi.org/10.14359/18624.

[11] B. S. Jang, B. H. Oh, Effects of non-uniform corrosion on the cracking and service life of reinforced concrete structures, Cement and Concrete Research 40 (9) (2010) 1441–1450. doi:https://doi.org/10.1016/j.cemconres.2010.03.018.

[12] U. Angst, B. Elsener, B. Jamali, A. Adey, Concrete cover cracking owing to reinforcement corrosion – Theoretical considerations and practical experience, Materials and Corrosion 63 (12) (2012) 1069–1077. doi:https://doi.org/10.1002/maco.201206669.

[13] A. Jamali, U. Angst, B. Adey, B. Elsener, Modeling of corrosion-induced concrete cover cracking: a critical analysis, Construction and Building Materials 42 (2013) 225–237. doi:https://doi.org/10.1016/j.conbuildmat.2013.01.019.

[14] P. Malumbela, G. Moyo, M. Alexander, A step towards standardising accelerated corrosion tests on laboratory reinforced concrete specimens, Journal of the South African Institution of Civil Engineering 54 (2) (2012) 78–85.

[15] A. Cesetti, G. Mancini, Tondolo, Pull-out tests on R.C. corroded specimens, in: F. Dehn, H.-D. Beushausen, M. G. Alexander, P. Moyo (Eds.), Proceedings of ICCRRR – International Conference on Concrete Repair, Rehabilitation and Retrofitting. 5-8 October 2015, CRC Press – Taylor and Francis Group, London, Leipzig, Germany, 2015, pp. 123–129.

[16] S. Coccia, S. Imperatore, Z. Rinaldi, Influence of corrosion on the bond strength of steel rebars in concrete, Materials and Structures 49 (1-2) (2016) 537–551. doi:https://doi.org/10.1617/s11527-014-0518-x.

[17] fib, fib Bulletin 10 – Bond of Reinforcement in Concrete, fib, 2000.

[18] C. Fang, K. Lundgren, L. Chen, C. Zhu, Corrosion influence on bond in reinforced concrete, Cement and Concrete Research 34 (2004) 2159–2167. doi:https://doi.org/10.1016/j.cemconres.2004.04.006.

[19] R. Al-Hammoud, K. Soudki, T. Topper, Bond analysis of corroded reinforced concrete beams under monotonic and fatigue loads, Cement and Concrete Composites 32 (3) (2010) 194–203. doi:https://doi.org/10.1016/j.cemconcomp.2009.12.001.

[20] British Standard Institution, BS4449:2005+A3:2016 Steel for the reinforcement of concrete – Weldable reinforcing steel – Bar, coil and decoiled product – Specification, British Standard Institution (BSI), London, United Kingdom, 2016.

[21] C. Alonso, C. Andrade, J. Rodriguez, M. Diez, Factors controlling cracking of concrete affected by reinforcement corrosion, Materials and Structures 31 (7) (1998) 435–441. doi:https://doi.org/10.1007/BF02480466.

[22] C. Alonso, C. Andrade, Corrosion rates of concretes made with different binders and exposed for 10 years in natural sea water, in: Proceedings of the 3rd RILEM Workshop on Testing and Modelling the Chloride Ingress into Concrete. 9-10 September 2002, Madrid, Spain, 2002, pp. 259–267. doi:https://doi.org/10.1617/2912143578.006.

[23] G. Mancini, F. Tondolo, Effect of bond degradation due to corrosion – A literature survey, Structural Concrete 15 (3) (2014) 408–418. doi:https://doi.org/10.1002/suco.201300009.

[24] C. Andrade, M. Alonso, J. Gonzalez, Corrosion rates of steel in concrete, in: N. Berke, V. Chaker, W. Whiting (Eds.), ASTM STP, Vol. 1065, Philadelphia, Pennsylvania, USA, 1990, p. 29.

[25] J. Gonzalez, C. Andrade, C. Alonso, S. Feliu, Comparison of rates of general corrosion and maximum pitting penetration on concrete

embedded steel reinforcement, Cement and Concrete Research 25 (2) (1995) 257–264. doi:https://doi.org/10.1016/0008-8846(95)00006-2.

[26] C. Andrade, C. Alonso, On-site measurements of corrosion rate of reinforcements, Construction and Building Materials 2 (15) (2001) 141–145. doi:https://doi.org/10.1016/S0950-0618(00)00063-5.

[27] J. Rodriguez, L. Ortega, M. Garcia, L. Johansson, K. Petterson, On site corrosion rate measurements in concrete structures using a device developed under the Eureka project EU-401, in: Proceedings of International Conference, Concrete Across Borders. 22-25 June 1994, Vol. 1, Odense, Denmark, 1994, pp. 215–226.

[28] C. Andrade, C. Alonso, J. González, J. Rodriguez, Remaining service life of corroding structures, in: Durability of Structures. IABSE Symposium, 6–8 September 1989 (IABSE Report Volume 57/1), Lisbon, Portugal, 1989, pp. 359–364.

[29] C. Andrade, C. Alonso, Corrosion rate monitoring in the laboratory and on-site, Construction and Building Materials 10 (5) (1996) 315–328. doi:https://doi.org/10.1016/0950-0618(95)00044-5.

[30] G. Cabrera, P. Ghodoussi, Discussion of Al-Sulaimani et al (1990), ACI Structural Journal 88 (1) (1991) 125–126.

[31] M. Saifullah, L. Clark, Effect of corrosion rate on the bond strength of corroded reinforcement, in: R. N. Swamy (Ed.), Proceedings of International Conference: Corrosion and Corrosion Protection of Steel in Concrete. 24-28 July 1994, Sheffield Academic Press, University of Sheffield, Sheffield, England, UK, 1994, pp. 591–602.

[32] D. Coronelli, Bond of corroded bars in confined concrete: test results and mechanical modeling, Studi e Ricerche, Politecnico di Milano 18 (1997) 187–209.

[33] S. S. Ayop, J. J. Cairns, The influence of impressed current on residual bond strength of corroded structure, Applied Mechanics and Materials 773 (2015) 984–989. doi:https://doi.org/10.4028/www.scientific.net/AMM.773-774.984.

[34] M. P. Webster, The assessment of corrosion-damaged concrete structures, Ph.D. thesis, University of Birmingham, England, UK (2000).

[35] P. S. Mangat, M. S. Elgarf, Flexural strength of concrete beams with corroding reinforcement, ACI Structural Journal 96 (1) (1999) 149–158. doi:https://doi.org/10.14359/606.

[36] G. Malumbela, M. Alexander, P. Moyo, Serviceability of corrosion-affected RC beams after patch repairs and FRPs under load, Materials and Structures 44 (1) (2011) 331–349. doi:https://doi.org/10.1617/s11527-010-9630-8.

[37] K. Sagoe-Crentsil, F. P. Glasser, Green rust, iron solubility and the role of chloride in the corrosion of steel at high pH, Cement and Concrete Research 23 (4) (1993) 785–791. doi:https://doi.org/10.1016/0008-8846(93)90032-5.

[38] C. Andrade, C. Alonso, F. J. Molina, Cover cracking as a function of bar corrosion: Part I – Experimental test, Materials and Structures 26 (8) (1993) 453–464. doi:https://doi.org/10.1007/BF02472805.

[39] J. G. Cabrera, Deterioration of concrete due to reinforcement steel corrosion, Cement and Concrete Composites 18 (1) (1996) 47–59. doi:https://doi.org/10.1016/0958-9465(95)00043-7.

[40] J. Rodriguez, L. M. Ortega, J. Casal, J. M. Diez, Corrosion of reinforcement and service life of concrete structures, in: C. Sjöström (Ed.), Proceedings of 7th International Conference on Durability of Building Materials and Components (DBMC 7). 1923 May 1996, Vol. 1, Stockholm, Sweden, 1996, pp. 117–126.

[41] A. A. Torres-Acosta, M. Martínez-Madrid, Residual life of corroding reinforced concrete structures in marine environment, Journal of Materials in Civil Engineering 15 (4) (2003) 344–353. doi:https://doi.org/10.1061/(ASCE)0899-1561(2003)15:4(344).

[42] T. Vidal, A. Castel, R. François, Analyzing crack width to predict corrosion in reinforced concrete, Cement and Concrete Research 34 (1) (2004) 165–174. doi:https://doi.org/10.1016/S0008-8846(03)00246-1.

[43] R. Zhang, A. Castel, R. François, Concrete cover cracking with reinforcement corrosion of RC beam during chloride-induced corrosion process, Cement and Concrete Research 40 (3) (2010) 415–425. doi:https://doi.org/10.1016/j.cemconres.2009.09.026.

[44] Y. Zhao, J. Yu, B. Hu, W. Jin, Crack shape and rust distribution in corrosion-induced cracking concrete, Corrosion Science 55 (2012) 385–393.

doi:https://doi.org/10.1016/j.corsci.2011.11.002.

[45] C. Andrade, A. Cesetti, G. Mancini, F. Tondolo, Estimating corrosion attack in reinforced concrete by means of crack opening, Structural Concrete 17 (4) (2016) 533–540. doi:https://doi.org/10.1002/suco.201500114.

[46] J. Cabrera, P. Ghodoussi, The effect of reinforcement corrosion on the strength of the steel/concrete bond, in: International Conference on Bond in Concrete: from Research to Practice. 15-17 October 1992, Vol. 3, Riga Technical University (RTU), Riga, Latvia, 1992, pp. 10–11.

[47] J. Rodriguez, L. Ortega, A. Garcia, Corrosion of reinforcing bars and service life of RC structures: corrosion and bond deterioration, in: Proceedings of International Conference, Concrete Across Borders. 22-25 June 1994, Vol. II, Danish Concrete Association, Odense, Denmark, 1994, pp. 315–326.

[48] P. Mangat, M. Elgarf, Bond characteristics of corroding reinforcement in concrete beams, Materials and Structures 32 (2) (1999) 89. doi:https://doi.org/10.1007/BF02479434.

[49] Y. Auyeung, P. Balaguru, L. Chung, Bond behavior of corroded reinforcement bars, Materials Journal 97 (2) (2000) 214–220. doi:https://doi.org/10.14359/826.

[50] K. Zandi Hanjari, D. Coronelli, K. Lundgren, Bond capacity of severely corroded bars with corroded stirrups, Magazine of concrete Research 63 (12) (2011) 953–968. doi:https://doi.org/10.1680/macr.10.00200.

[51] C. Fischer, J. Ožbolt, Influence of bar diameter and concrete cover on bond degradation due to corrosion, in: J. Cairns, G. Metelli, G. Plizzari (Eds.), Proceeding of 4th international Symposium: Bond in concrete 2012: Bond, Anchorages, Detailing. 17-20 June 2012, Brescia, Italy, 2012, pp. 445–451.

[52] M. Tahershamsi, I. Fernandez, K. Lundgren, K. Zandi, Investigating correlations between crack width, corrosion level and anchorage capacity, Structure and Infrastructure Engineering 13 (10) (2017) 1294–1307. doi:https://doi.org/10.1080/15732479.2016.1263673.

[53] C. A. Apostolopoulos, K. F. Koulouris, A. C. Apostolopoulos, Correlation of surface cracks of concrete due to corrosion and bond strength (between steel bar and concrete), Advances in Civil Engineering 2019 (2019) 1–12. doi:https://doi.org/10.1155/2019/3438743.

[54] M. Berra, A. Castellani, D. Coronelli, Bond in reinforced concrete and corrosion of bars, in: M. C. Forde (Ed.), Proceedings of the 7th International Conference on Structural Faults and Repair. Volume 2: Concrete and Composites. 8 July 1997, Vol. 2, Engineering Technics Press, University of Edinburgh, Scotland, UK, 1997, pp. 349–356.

[55] H.-S. Lee, T. Noguchi, F. Tomosawa, Evaluation of the bond properties between concrete and reinforcement as a function of the degree of reinforcement corrosion, Cement and Concrete research 32 (8) (2002) 1313–1318. doi:https://doi.org/10.1016/S0008-8846(02)00783-4.

[56] H. Yalciner, O. Eren, S. Sensay, An experimental study on the bond strength between reinforcement bars and concrete as a function of concrete cover, strength and corrosion level, Cement and Concrete Research 42 (2012) 643–655. doi:https://doi.org/10.1016/j.cemconres.2012.01.003.

[57] C. Fischer, J. Ožbolt, C. Gehlen, Numerical investigation on bond behavior of corroded reinforcement, in: B. H. Oh (Ed.), Proceedings of 7th International Conference on Fracture Mechanics of Concrete and Concrete Structures (FraMCoS-7). 22-27 May 2010, Korea Concrete Institute, Jeju, South Korea, 2010, pp. 779–785.

[58] D. W. Law, D. Tang, T. K. Molyneaux, R. Gravina, Impact of crack width on bond: confined and unconfined rebar, Materials and structures 44 (7) (2011) 1287–1296. doi:https://doi.org/10.1617/s11527-010-9700-y.

[59] H. Lin, Y. Zhao, J. Ožbolt, R. Hans-Wolf, The bond behavior between concrete and corroded steel bar under repeated loading, Engineering Structures 140 (2017) 390–405. doi:https://doi.org/10.1016/j.engstruct.2017.02.067.

[60] P. G. Gambarova, G. P. Rosati, B. Zasso, Steel-to-concrete bond after concrete splitting: test results, Materials and Structures 22 (1) (1989) 35–47. doi:https://doi.org/10.1007/BF02472693.

[61] P. Desnerck, J. M. Lees, C. T. Morley, Bond behaviour of reinforced concrete bars in cracked concrete, Construction and Building Materials 94 (2015) 126–136. doi:https://doi.org/10.1016/j.conbuildmat.2015.06.043.

[62] fib, fib Model Code for Concrete Structures 2010, Ernst and Sohn, Berlin, Germany, 2013. doi:http://doi.org/10.1002/9783433604090.

[63] RILEM, Essais portant sur l'adhérence des armatures du béton – 2. Essai par traction. (French) [Bond test for reinforcing steel – 2. Pull-out test], Matériaux et Construction 3 (15) (1970) 175–178. doi:https://doi.org/10.1007/BF02478968.

[64] European Committee for Standardisation, EN 12390-3:2009 Testing hardened concrete – Part 3: Compressive strength of test specimens, European Committee for Standardisation (CEN), Brussels, Belgium, 2009.

[65] European Committee for Standardisation, EN 12390-6:2009 Testing hardened concrete – Part 6: Tensile splitting strength of test specimens, European Committee for Standardisation (CEN), Brussels, Belgium, 2009.

[66] A. Horne, I. Richardson, R. Brydson, Quantitative analysis of the microstructure of interfaces in steel reinforced concrete, Cement and Concrete Research 37 (12) (2007) 1613–1623. doi:https://doi.org/10.1016/j.cemconres.2007.08.026.

[67] T. A. Soylev, R. François, Quality of steel–concrete interface and corrosion of reinforcing steel, Cement and Concrete Research 33 (9) (2003) 1407–1415. doi:https://doi.org/10.1016/S0008-8846(03)00087-5.

[68] U. Angst, Chloride induced reinforcement corrosion in concrete: Concept of critical chloride content–methods and mechanisms, Ph.D. thesis, Norwegian University of Science and Technology, Trondheim, Norway (2011).

[69] U. Angst, Ø. Vennesland, C. Larsen, B. Elsener, Chloride induced reinforcement corrosion: results from a laboratory study within the norwegian COIN project, in: H. Justnes, S. Jacobsen (Eds.), Proceedings of the International Congress on Durability of Concrete. 18-21 June 2012, Trondheim, Norway, 2012, p. 116.

[70] F. Molina, C. Alonso, C. Andrade, Cover cracking as a function of rebar corrosion: Part 2 – Numerical model, Materials and Structures 26 (9) (1993) 532–548. doi:https://doi.org/10.1007/BF02472864.

[71] D. Coronelli, Corrosion cracking and bond strength modeling for corroded bars in reinforced concrete, ACI Structural Journal 99 (3) (2002) 267–276. doi:https://doi.org/10.14359/11910.

[72] S. Masoud, K. Soudki, T. Topper, CFRP-strengthened and corroded RC beams under monotonic and fatigue loads, Journal of composites for construction 5 (4) (2001) 228–236. doi:https://doi.org/10.1061/(ASCE)1090-0268(2001)5:4(228).

[73] G. Malumbela, M. Alexander, P. Moyo, Interaction between corrosion crack width and steel loss in RC beams corroded under load, Cement and Concrete research 40 (9) (2010) 1419–1428. doi:https://doi.org/10.1016/j.cemconres.2010.03.010.

[74] S. H. Chu, A. K. H. Kwan, A new method for pull out test of reinforcing bars in plain and fibre reinforced concrete, Engineering Structures 164 (2018) 82–91. doi:https://doi.org/10.1016/j.engstruct.2018.02.080.

[75] R. Tepfers, Cracking of concrete cover along anchored deformed reinforcing bars, Magazine of Concrete Research 31 (106) (1979) 3–12. doi:https://doi.org/10.1680/macr.1979.31.106.3.

[76] M. W. T. Mak, P. Desnerck, J. M. Lees, Data supporting: Corrosion-induced cracking and bond strength in reinforced concrete (2019). doi:https://doi.org/10.17863/CAM.37247.